

UC Irvine

UC Irvine Previously Published Works

Title

Evaluation of Bilayer Silk Fibroin Grafts for Tubular Esophagoplasty in a Porcine Defect Model

Permalink

<https://escholarship.org/uc/item/0dh0d1qr>

Journal

Tissue Engineering Part A, 27(1-2)

ISSN

1937-3341

Authors

Gundogdu, Gokhan
Morhardt, Duncan
Cristofaro, Vivian
et al.

Publication Date

2021

DOI

10.1089/ten.tea.2020.0061

Peer reviewed

Evaluation of Bi-layer Silk Fibroin Grafts for Tubular Esophagoplasty in a Porcine Defect Model

Gokhan Gundogdu¹, Duncan Morhardt^{2,3}, Vivian Cristofaro^{3,4,5}, Khalid Algarrahi^{2,3}, Xuehui Yang^{2,3}, Kyle Costa^{2,3}, Cinthia Galvez Alegria^{2,3}, Maryrose P. Sullivan^{3,4,5}, Joshua R. Mauney^{1,§}

¹Departments of Urology and Biomedical Engineering, University of California, Irvine, Orange, CA 92868, USA.

²Urological Diseases Research Center, Boston Children's Hospital, Boston, MA 02115, USA.

³Department of Surgery, Harvard Medical School, Boston, MA 02115, USA.

⁴Division of Urology, Veterans Affairs Boston Healthcare System, Boston, MA 02132, USA

⁵Department of Surgery, Brigham and Women's Hospital, Boston, MA 02115, USA.

§Corresponding author: Joshua R. Mauney, Ph.D., University of California, Irvine, Department of Urology and Biomedical Engineering, Building 55, 101 The City Drive South., Rm. 300, Orange, CA 92868, USA; Phone: 714-456-6489; email: mauneyj@hs.uci.edu

Contact information for other authors:

Dr. Gokhan Gundogdu: University of California, Irvine, Department of Urology, Building 55, 101 The City Drive South., Rm. 300, Orange, CA 92868; Phone: 714-456-6782; email: ggundogd@hs.uci.edu.

Dr. Duncan Morhardt: Boston Children's Hospital, Department of Urology, John F. Enders Research Laboratories, 300 Longwood Ave., Rm. 1013, Boston, MA 02115; Phone: 617-919-2520; email: Duncan.Morhardt@childrens.harvard.edu.

Dr. Vivian Cristofaro: Boston VA Medical Center, Department of Urology, Building 3, Rm. 2C108, 1400 VFW Pkwy, West Roxbury, MA 02132; Phone: 617-323-7700; email: Vivian_Cristofaro@hms.harvard.edu.

Dr. Khalid Algarrahi: Boston Children's Hospital, Department of Urology, John F. Enders Research Laboratories, 300 Longwood Ave., Rm. 1013, Boston, MA 02115; Phone: 617-919-2520; email: kalgarrahi@gmail.com.

Ms. Xuehui Yang: Boston Children's Hospital, Department of Urology, John F. Enders Research Laboratories, 300 Longwood Ave., Rm. 1017, Boston, MA 02115; Phone: 617-919-6942; email: xuehui.yang@childrens.harvard.edu.

Mr. Kyle Costa: Boston Children's Hospital, Department of Urology, John F. Enders Research Laboratories, 300 Longwood Ave., Rm. 1017, Boston, MA 02115; Phone: 617-919-6942; email: kyle.costa@childrens.harvard.edu.

Dr. Cinthia Galvez Alegria: Boston Children's Hospital, Department of Urology, John F. Enders Research Laboratories, 300 Longwood Ave., Rm. 1013, Boston, MA 02115; Phone: 617-919-2520; email: cinthiagal@icloud.com.

Dr. Maryrose P. Sullivan: Boston VA Medical Center, Department of Urology, Building 3, Rm. 2C108, 1400 VFW Pkwy, West Roxbury, MA 02132; Phone: 617-323-7700; email: msullivan@rics.bwh.harvard.edu.

Short running title: Silk Fibroin Grafts for Esophagoplasty

Key words: esophagus, silk fibroin scaffolds, tissue engineering

Abstract

Surgical reconstruction of tubular esophageal defects with autologous gastrointestinal segments is the gold standard treatment to replace damaged or diseased esophageal tissues. Unfortunately, this approach is associated with adverse complications including dysphagia, donor site morbidity and in some cases patient death. Bi-layer silk fibroin (BLSF) scaffolds were investigated as alternative, acellular grafts for tubular esophagoplasty in a porcine defect model for 3 months of implantation. Adult Yucatan mini-swine (N=5) were subjected to esophageal reconstruction with tubular BLSF grafts (2 cm in length) in combination with transient esophageal stenting for 2 months followed by a 1 month period where the graft site was unstented. All animals receiving BLSF grafts survived and were capable of solid food consumption, however strictures were noted at graft regions in 60% of the experimental cohort between 2-3 months post-op and required balloon dilation. In addition, fluoroscopic analysis showed peristaltic function in only 1/5 neotissues. Following swine harvest at 3 months, *ex vivo* tissue bath evaluations revealed neoconduits exhibited contractile responses to carbachol, electric field stimulation, and KCl while sodium nitroprusside and isoproterenol induced relaxation effects. Histological (Masson's trichrome) and immunohistochemical analyses of regenerated tissue conduits showed a stratified, squamous epithelium expressing pan-cytokeratins buttressed by a vascularized lamina propria containing a smooth muscle-rich muscularis mucosa surrounded by a muscularis externa. Neuronal density, characterized by the presence of synaptophysin-positive boutons, was significantly lower in neotissues in comparison to nonsurgical controls. BLSF scaffolds represent a promising platform for the repair of tubular esophageal defects, however improvements in scaffold design are needed to reduce the rate of complications and improve the extent of constructive tissue remodeling.

Impact Statement

The search for a superior “off-the-shelf” scaffold capable of repairing tubular esophageal defects as well as overcoming limitations associated with conventional autologous gastrointestinal segments remains elusive. The purpose of this study was to investigate the performance of an acellular, bi-layer silk fibroin graft (BLSF) graft for tubular esophagoplasty in a porcine model. Our results demonstrated that BLSF scaffolds supported the formation of tubular neotissues with innervated, vascularized epithelial and muscular components capable of contractile and relaxation responses. BLSF scaffolds represent a promising platform for esophageal tissue engineering.

Introduction

Tubular esophageal defects resulting from esophageal atresia, tracheoesophageal fistula, malignancy, Barrett's esophagus, and caustic ingestion represent life-threatening afflictions which require surgical intervention to restore organ continuity and allow for passage of food and liquids (1-5). Replacement of developmentally absent or diseased esophageal tissues is conventionally accomplished with gastric pull-up or colonic interposition grafts (6). However, these strategies have been associated with high rates of neotissue dysmotility (5-25%), donor site morbidity (26-55%) and patient mortality (3-6%) (7-11). Mechanical traction to encourage elongation of distant esophageal segments for treatment of esophageal atresia has also been explored via the Foker technique. Unfortunately, extensive hospitalization as well as complication rates up to 80% have been reported (12). These studies highlight the need for novel strategies for tubular esophagoplasty which can minimize unwanted side-effects and promote functional tissue regeneration. Currently, there is no FDA-approved tissue engineered device for esophageal tissue replacement.

Biodegradable matrices composed of decellularized tissues, collagen or synthetic polymers such as polyurethane and polyesters have been previously investigated as potential alternatives to autologous tissue grafts for esophageal repair (13). These biomaterials have been utilized alone or seeded with primary keratinocytes or mesenchymal stem cell populations for reconstruction of partial and full circumferential esophageal defects in both animal models and in some cases short-term clinical trials (14-27). Despite the ability of these tissue engineered constructs to support constructive remodeling following onlay esophagoplasty, suboptimal outcomes including stricture formation and graft perforation have been reported following restoration of tubular esophageal segments (14, 18, 20, 22). Dilation and covered stenting are commonly used methods to preserve esophageal continuity during scaffold-mediated, wound healing, however fibrosis and abnormal tissue function are still frequently observed in *de novo* conduits (15, 25). Advancements in esophageal tissue engineering are dependent on new biomaterial configurations which can preserve organ function while promoting host regenerative responses.

In the present study, we hypothesized that acellular, bi-layer silk fibroin (BLSF) scaffolds can facilitate functional regeneration of tubular esophageal defects. Protein-based, BLSF biomaterials were designed to reinforce hollow organ defects while gradually dissipating and allowing for host tissue ingrowth and subsequent regeneration of native tissue structure and function (28-31). The bi-layer matrix is composed of *Bombyx mori* silk fibroin protein fashioned into a film layer and then annealed to a foam compartment, the former provides a fluid-tight seal, mechanical strength, and bulk scaffold suturability while the latter creates a microenvironment for neotissue formation (28, 30).

BLSF grafts offer several advantages over conventional decellularized tissue matrices and synthetic polymer-based scaffolds previously used for esophageal tissue reconstruction. For example, BLSF biomaterials represent a tunable biomaterial platform wherein their structural, mechanical, and degradative properties can be adjusted by manipulating fabrication parameters such as silk fibroin content and porogen size in order to optimize wound healing responses (28-31). These physical attributes contrast with decellularized tissue matrices which are dependent upon the characteristics of the source tissue as well as the processing protocols utilized for decellularization (32). In addition, BLSF grafts are less immunogenic than polyester meshes since they degrade into naturally occurring amino acids and therefore do not elicit adverse foreign body reactions commonly seen with the degradation metabolites of synthetic polymers (33, 34).

Our previous reports have demonstrated that acellular BLSF scaffolds can support constructive remodeling of patch esophageal defects in both small and large animal models of surgical damage and corrosive strictures (29-31). In comparison to decellularized tissue grafts, BLSF matrices generate less graft site contracture, elicit minimal inflammatory reactions and fibrosis, and promote higher degrees of muscular and neuronal regeneration at esophageal implant sites (29). In the current work, we examined the efficacy of BLSF grafts for tubular esophagoplasty in a porcine defect model.

Material and methods

Biomaterials

BLSF scaffolds were cast from processed silk fibroin solutions derived from *B. mori* cocoons using previously described methods (28). Structural and mechanical properties of

BLSF matrices have been reported in past studies (30). Biomaterial strips were steam sterilized and then aseptically fashioned into tubes (1.5 cm in diameter, 2 cm in length) with 4-0 propylene sutures prior to surgery.

Surgical Procedures

All *in vivo* experiments were performed under protocol 17-10-3555R following approval by the Boston Children's Hospital Animal Care and Use Committee. Animal manipulations were carried out following the recommendations from the National Institutes of Health Guide for the Care and Use of Laboratory Animals. BLSF grafts were assessed in a tubular esophagoplasty model using adult, Yucatan mini-swine (N=10, ~30–40 kg, Sinclair Bio Resources LLC, Windham ME) for 3-4 months of implantation (**Figure 1**). A pilot study was initially performed with 5 swine (Pigs A-E, one male, four female) to determine the ability of BLSF matrices to support defect consolidation alone or with various periods of esophageal stenting. Following these experiments, a second group of 5 swine (Pigs 1-5, all female) were investigated with a surgical approach optimized from our pilot experience. Female subjects were predominantly included in our experimental cohorts due to the absence of a subcutaneous shield plate which hinders surgical access to the thoracic cavity in males.

Overall, swine were fasted 12 hours before operative procedures with free access to water. All experiments were performed under general anesthesia, initiated by intramuscular injection of 0.4 mg/kg atropine, 2.2 mg/kg xylazine and 4.4 mg/kg tiletamine+zolazepam, and sustained with 1-4% isoflurane inhalation through an endotracheal tube. A gastrostomy (G-) tube was first placed in all animals to allow for enteral feeding during initial stages of defect consolidation. Specifically, swine were placed in the supine position and a stomach tube (Portex®, Jorgensen Laboratories, Inc. CO) was introduced orally under guidance with a flexible endoscope (Olympus GIF130, Tokyo, Japan). Following abdominal incision, a Stamm gastrostomy was created in the anterior stomach wall using a 5 cm, 24 Fr button-gastrostomy catheter. The stomach tube was pulled out and the wound was closed in layers and dressed.

For esophageal reconstruction, the lower esophagus was approached by a transpleural thoracotomy through the right 7th and 8th intercostal region. The mediastinal pleura was opened vertically, and a 2 cm distal esophageal segment located 5 cm above the lower esophageal sphincter line was resected with preservation of the vagal nerve. A tubular BLSF graft of equal length was sutured to the proximal and distal stumps of the esophagus by using absorbable 4-0 monofilament polyglactin sutures. The anastomotic edges were marked with non-absorbable 4-0 propylene sutures to identify the boundaries of the original implant site. In addition, scaffold margins and the esophagogastric junction were also demarcated with radiopaque beads to allow targeting of the implant region during radiographic studies. For stent deployment, an endoscope was again inserted into the stomach and a guide-wire (Dreamwire™ Boston Scientific, MA) was introduced through the working channel and left in the esophagus. A 100 x 18 mm, fully covered esophageal stent (Wallflex M00516210, Boston Scientific, MA) was then deployed into the esophagus under fluoroscopy and positioned to reinforce the scaffold implantation site. In aim to prevent stent migration, the upper edge of the esophagus stent was tethered to the esophageal wall by an absorbable 2-0 chromic catgut U-stitch under endoscopic surveillance. The esophagus was then covered by suturing the mediastinal pleura and a chest tube was installed and sealed. The thoracotomy incision was closed in layers and the chest tube removed. Post-operative pain was managed by intercostal Bupivacaine HCl 0.25% (1-3 mg/kg) infiltration prior to rib approximation as well as an intramuscular injection of 1.1 mg/kg banamine and a transdermal 4 µg/kg fentanyl patch for 72 hours. Animals were recovered in a warm incubator until they became sternal.

Swine were weighed preoperatively and once a week over the course of the study. Animals were nourished by enteral food slurry consisting of diluted pig feed mixed with PediaSure® (Abbott Laboratories, Columbus, OH) for 1 week post-op via G-tube administration. Animals were then transitioned to oral feedings of standard pig chow over the course of 3-7 days and maintained on an oral diet for the remainder of the study. Radiographic imaging was performed at baseline and weekly from 1 to 2 months after grafting to monitor esophageal continuity and stent position. At the 2 month timepoint, stents were removed and graft sites were evaluated by endoscopic and fluoroscopic

methods. Animals were intermittently monitored at least twice daily for indications of esophageal stenosis including significant weight loss, prolonged feeding time, or excessive oral salivation. In cases where esophageal stricture formation was detected during endoscopic surveillance, balloon dilation was performed to widen organ caliber and animals were placed back on oral feeding for the duration of the study.

All animals were survived for a total of 2-4 months and evaluated by radiographic and endoscopic analyses prior to sacrifice with an intravenous Fatal-Plus infusion (100mg/kg; Vortech Pharmaceutical, MI). Following necropsy, regenerated conduits were excised from host tissues and divided axially into four circumferential rings (~7-8 mm in length) representing 2 peripheral (adjacent to anastomotic border) and 2 central zones of neotissue. Tissue specimens from both central and peripheral regions were analyzed for outcome analyses described below. Tubular esophageal segments excised 5 cm above the scaffold implantation site were evaluated in parallel as internal proximal controls. In addition, native esophageal tissues that were excised to create the defect for graft implantation were assessed similarly as nonsurgical controls (NSC).

Esophagoscopy

All endoscopic procedures were performed under general anesthesia. Swine were positioned on their left lateral side, and the airway was secured with an endotracheal tube to avoid the aspiration. A flexible endoscope (Olympus® GIF130, Tokyo, Japan) was then advanced over the tongue and oropharynx to the implant site where the mucosal surface was evaluated at study timepoints. Images were obtained with an Olympus® video processor (Olympus® CV-100 video processor, Tokyo, Japan).

Radiologic imaging: Esophagrams and Fluoroscopy

Barium esophagram and fluoroscopic assessments were carried out on swine preoperatively and at selective experimental timepoints described above following BLSF graft implantation to evaluate neoconduit continuity, function, the presence of strictures or fistulas, as well as stent position. Contrast agents including Gastrografin® (diatrizoate meglumine and diatrizoate sodium solution USP, Bracco, Monroe Township, NJ) or E-Z-EM® LIQUID E-Z-PAQUE Barium Sulfate suspension (E-Z-EM, Inc., NY) were instilled in the

proximal esophagus via a stomach tube. Lateral fluoroscopy was performed during contrast agent transit with an ADC/XRE Unicath SP fluoroscopy instrument (XRE Corporation, MA) and lateral and anterior/posterior (AP) esophagrams were acquired using an AMX-4 portable X-ray machine (General Electric, CT). Neotissues were identified with radiopaque markers positioned at the time of grafting.

Ex Vivo tissue contractility and relaxation responses

Denuded esophageal tissue strips isolated from BLSF graft sites at 3 months post-op (N=5), unoperated proximal controls (N=5), and NSC (N=4) were evaluated in tissue baths for *ex vivo* contractility/relaxation responses. Tissue specimens were equilibrated at a resting tension of 2 grams and testing was performed in Krebs's solution at 37°C aerated with carbogen. Esophageal contractile responses were induced by exogenous administration of KCl (120 mM) or muscarinic receptor agonist carbachol (10 μ M). Relaxation responses were evoked in tissues pre-contracted with carbachol by administration of β -adrenoceptor agonist, isoproterenol (10 μ M) or nitric oxide donor, sodium nitroprusside (SNP, 10 μ M). In addition, the response to electrical field stimulation (EFS, 0.5-20 Hz, 0.5 ms pulse duration, 16V, 10 s) was determined in carbachol, pre-contracted tissue. In the normal esophagus, EFS of circular esophageal smooth muscle produces a small frequency-dependent response during stimulation (on-contraction) followed by a more pronounced contraction once the stimulus is terminated (off-contraction). Frequency-response curves were therefore generated from the force of the on-contraction measured during stimulation, as well as the amplitude of the post-stimulation off-contraction. Tension force generated from evoked responses was normalized to sample area.

Histological, immunohistochemical (IHC), and histomorphometric analyses

Tubular esophageal specimens from central and peripheral regions of neotissues (N=5), proximal controls (N=5), and NSC (N=4) were excised from swine following euthanasia, fixed in 10% neutral-buffered formalin, subjected to alcohol dehydration, and embedded in paraffin. Sections (5 μ m) were stained with Masson's trichrome, digitally imaged across the entire section, and collagen content was determined with a color

segmentation program in ImageJ using previously reported methods (35) to quantify blue-stained color elements indicative of collagen deposition. Collagen content was calculated as the percentage of blue stained area (collagen) per total field area examined.

IHC evaluations were carried out on parallel tissue sections after antigen retrieval in 10 mM sodium citrate buffer (pH 6.0) and incubation in blocking buffer consisting of PBS with 5% fetal bovine serum, 1% BSA, and 0.3% Triton X-100 for 1 hr at room temperature. Specimens were probed with the following primary antibodies overnight at 4°C: anti-pan-cytokeratin (CK) [Dako, Carpinteria, CA, 1:150 dilution], anti- α -smooth muscle actin (SMA) [Sigma-Aldrich, St. Louis, MO, 1:200 dilution], anti-slow skeletal myosin heavy (MYH) [Abcam, Cambridge, MA, 1:200 dilution], anti-CD31 [Abcam, 1:100 dilution], and anti-synaptophysin (SYP) [Abcam, 1:50 dilution]. Specimens were then stained with species-matched Alexa Fluor 488 and 594-conjugated secondary antibodies (Thermo Fisher Scientific, Waltham, MA) and nuclei were counterstained with 4', 6-diamidino-2-phenylindole (DAPI). Specimen visualization was performed with an Axioplan-2 microscope (Carl Zeiss MicroImaging, Thornwood, NY) and representative fields were acquired with Axiovision software (version 4.8). Negative controls consisting of parallel specimens stained with secondary antibodies in the absence of primary antibodies were performed similarly and produced no detectable signal above background.

Histomorphometric analyses (N=4-5 animals per group) were carried out on 4 independent microscopic fields (20X magnification) equally dispersed along the circumference of each reconstructed and control tubular specimen using published protocols (30). Specifically, area measurements and image thresholding were performed on microscopic fields with ImageJ software (version 1.47) to determine the percentage of tissue area stained for MYH, α -SMA, and pan-CK per total field area evaluated. Numbers of SYP+ boutons and CD31+ vessels were calculated across 4 independent microscopic fields (10X and 20X magnifications for CD31 and SYP, respectively) per specimen using similar methods and normalized to total field area to determine neuronal and vascular density.

Statistical analyses

Statistical evaluations of quantitative measurements were performed using the Kruskal-Wallis test in combination with post hoc Dunn's test for pairwise comparisons,

considering a value of $p < 0.05$ as significant. Quantitative data were displayed as means \pm standard deviation unless otherwise indicated.

Results

A total of 5 swine were utilized in pilot studies (Pigs A-E) to refine our tubular esophagoplasty approach (**Table 1**). Barium esophagrams and fluoroscopic assessments were performed throughout the study period to monitor esophageal continuity and function (**Supplementary Figure S1A**). Studies with an unstented pilot animal (Pig A) revealed that the BLSF matrix supported initial defect consolidation with no contrast extravasation noted in barium esophagrams for up to 4 weeks of scaffold implantation. However, a severe stricture was observed at 5 weeks post-op which was associated with changes in animal behavior such as excessive salivation and esophageal dysphagia. This animal was treated with repeated balloon dilation and survived for a total of 4 months. Pig B was treated with a partially covered esophageal stent at the time of BLSF graft integration and stent removal was performed at 1 month post-op. A stricture was also noted at 5 weeks after esophageal reconstruction via esophagrams and balloon dilation was performed to restore esophageal continuity. A new stent was placed into the esophagus and maintained for additional 2 months until animal harvest. Tissue ingrowth into the stent at the terminal timepoint prevented removal which limited imaging assessments of peristaltic function in the neotissue. Three additional pilot swine (Pigs C-E) were studied wherein tubular esophagoplasty with BLSF matrices was performed in combination with initial stent placement and a stent exchange at 1 month to prevent tissue ingrowth. Stent migration into the stomach occurred in all swine between 1-2 months post-op with stricture formation observed between 1-3 months post-reconstruction. Pigs C and D were harvested at 3 months following scaffold implantation, while Pig E was sacrificed at approximately 2 months post-op due to severe esophageal dysphagia and stricture formation. Peristaltic contractions were noted in neotissues from Pigs C and D at the end of the study period following barium challenge. Upon necropsy, host tissue ingrowth was present throughout the original graft site in all pilot swine with negligible axial contraction of the implant region observed (**Supplementary Figure S2**).

Given our pilot study experience, tubular esophagoplasty with BLSF scaffolds was carried out in 5 subsequent animals (Figs 1-5) utilizing a transient, tethered fully covered stent deployed at the time of tissue repair to prevent migration (**Table 2**). Stents were then removed at 2 months and animals were monitored for a total of 3 months post-op until sacrifice. All 5 swine subjected to this surgical approach survived until scheduled euthanasia at 3 month post-op. No significant weight loss was encountered in swine at time of harvest (34 ± 5 kg) in comparison to pre-operative levels (34 ± 3 kg). Animals were capable of oral food consumption after 1 week of enteral feeding with no clinical signs of esophageal dysphagia, vomiting, or excessive salivation observed over the course of 2 months. Stent position in all animals was maintained at the site of esophageal reconstruction until endoscopic retrieval. Following stent removal at 2 months post-op, radiographic esophagrams (**Figure 2** and **Supplementary Figure S1B**) noted varying degrees of dilation in all reconstructed conduits relative to the adjacent host esophageal tissues, while endoscopic surveillance revealed mucosal regeneration had been achieved throughout the original implant region. In 3 out of 5 animals, excessive salivation and vomiting were noted 1-3 weeks following stent removal. Fluoroscopic and endoscopic evaluations confirmed stricture formation in the implant center of two swine and in the host tissues adjacent to the stent flares in another pig. Therefore, the incidence of stricture formation associated with matrix grafting in combination with transient stenting was 60%. Esophageal continuity was restored in each of these animals following balloon dilation and subjects were capable of oral intake of food and liquids until harvest at 3 months post-op. Endpoint analyses at the terminal timepoints revealed mild dilation in all reconstructed esophageal segments relative to the adjacent host esophageal tissues, however only 1 out of 5 neoconduits displayed peristaltic contractions following barium challenge.

Gross tissue assessments (**Figure 3**) at 3 months post-op necropsy demonstrated host tissue ingrowth throughout the original graft site in Figs 1-5. Neotissues exhibited minimal axial contraction between the proximal/distal marking sutures and no mucosal ulceration was observed. Mild abdominal adhesions were present on the exterior of all graft sites. Global histological evaluations (**Figure 4**) of the neoconduit peripheries (~7-8 mm from the anastomotic borders) revealed a cross-sectional architecture similar to NSC.

Regenerated mucosa consisted of a vascularized lamina propria lined with a stratified, squamous epithelium. In addition, *de novo* muscle components were organized into a smooth muscle-rich, muscularis mucosa surrounded by circular and longitudinal layers of striated skeletal and smooth muscle bundles. Central regions of the neotissues were also epithelialized, however muscle formation in the *de novo* esophageal wall was underdeveloped and consisted of discontinuous patches of muscle bundles. Mean collagen content was found to be highly variable among neotissue segments (periphery: $22\pm 6\%$; center: $23\pm 20\%$), nonetheless regenerated tissues displayed elevated levels of ECM deposition in comparison to NSC ($13\pm 2\%$). Scattered mononuclear inflammatory cells were seen throughout the center of neoconduits and were generally associated with areas of ongoing tissue remodeling. Minute scaffold fragments were occasionally observed in regenerated tissues; however, the main bulk of the graft had dissipated by 3 months of implantation.

IHC (**Figure 5**) and histomorphometric (**Figure 6**) evaluations were performed on Pigs 1-5 to assess the degree of neotissue maturation with respect to native esophageal tissues. The level of pan-CK+ epithelia was consistent throughout the length of neoconduits and the degree of immunoreactivity was similar between NSC, proximal-controls and surgical cohorts. The vessel density of regenerated tissues was overall significantly higher compared to NSC levels. Increased vascularization at graft sites has been associated with active wound healing processes suggesting neotissues at 3 months were still undergoing maturation (30, 36). Moreover, neotissue innervation, as demonstrated with SYP staining, was found to be incomplete with significantly lower neuronal density detected in neotissues in respect to NSC. In comparison to NSC, proximal-controls displayed significantly elevated vessel density in combination with significantly reduced neuronal density which could be indicative of ongoing repair processes from tissue damage incurred from operative procedures or stent deployment. A *de novo* muscularis mucosa was present in all neoconduit segments with levels of α -SMA+ smooth muscle bundles in line with NSC and proximal-controls. In contrast, the muscularis externa in the *de novo* esophageal walls displayed significantly elevated ratios of smooth to skeletal muscle (periphery: 4.5; center: 85) in respect to NSC (0.23). Interestingly, the central regions of the neoconduits were predominantly composed of α -SMA+ smooth

muscle and contained the lowest level of MYH+ skeletal muscle fibers in respect to all other experimental groups. In addition, unoperated proximal control tissues displayed a smooth to skeletal muscle ratio of 1.5.

Ex vivo tissue bath studies were performed to characterize the contractile/relaxation responses of control and regenerated tissues. Peripheral and central regions of neoconduits displayed similar levels of force generation as control groups in response to KCl and carbachol (**Figure 7A**). Consistent with our previous studies (30), carbachol pre-contracted neotissues from grafted sites displayed a greater relaxation in response to isoproterenol compared to NSC, with the graft periphery being significantly higher than NSC. Relaxation responses to sodium nitroprusside were not different among groups (**Figure 7B**). *De novo* tissues also exhibited frequency-dependent, on-contractile and on-relaxation responses as well as off-contractions following EFS (**Figure 7C, D**). At selective frequencies, neotissues displayed significantly lower on-contractions in respect to NSC, however there was no significant difference between responses in specimens isolated from the periphery or center. In addition, off-contractile responses were also found to be significantly muted in comparison to NSC with regional variations detected between central and peripheral segments.

Discussion

The aim of this report was to investigate the use of acellular BLSF grafts for tubular esophagoplasty in a porcine model of full thickness, circumferential tissue resection. Cell-free biomaterials were explored since they offer distinct advantages over cell-seeded scaffolds for esophageal tissue engineering such as “off-the-shelf” accessibility, lack of secondary surgeries to acquire host cells for construct seeding, and dispensability of specialized tissue culture facilities for construct maturation. Swine were used as a model species for our experiments given their omnivorous diet and comparable anatomy to humans (37). Tubular esophageal defects are present in both pediatric and adult patient populations, however we chose to explore developmentally mature animals in our assessments to simulate adult clinical repair settings wherein wound healing efficiency is impacted by age and growth-related changes in the esophagus are minimal (35, 38).

Overall, our results demonstrated that BLSF matrix conduits in combination with transient stenting supported the formation of innervated, vascularized esophageal tissues with contractile/relaxation properties. Stricture formation in reconstructed esophageal tissues was a limitation in the scaffold technology, however stricture rates were reduced from 100% to 60% following a 2 month stenting period. Refinements to our surgical approach included the use of tethered stents which allowed the device to be maintained at the graft site until scheduled removal. Transient stenting of reconstructed conduits has been previously used in combination with both acellular and cell-seeded constructs to mitigate early esophageal stenosis (15, 25). Moreover, the duration of stent deployment has also been shown to play a major role in determining stricture risk (15). These findings are consistent with our data and suggest that stent reinforcement is necessary to maintain the integrity of the remodeling esophageal wall during the initial phases of wound healing. Recent studies of cell seeded, polymer mesh-based conduits have reported stenting periods of 6 months or longer were required to eliminate stricture occurrence up to 1 year following stent removal (25). It remains to be seen if prolonged stenting periods can further reduce the rate of stricture at BLSF graft sites. Finally, our longitudinal observations highlight the need to perform functional evaluations of *de novo* tissues following stent removal since latent stricture formation and motility issues can arise in unsupported implant sites.

Wound healing patterns and functional properties of neotissues following tubular esophagoplasty exhibited both similarities and differences with our previous study of BLSF matrices in a porcine model of patch esophagoplasty (30). Stricture incidence was a major difference between the experimental outcomes of patch versus tubular esophageal reconstruction with unstented onlay grafts supporting *de novo* tissue ingrowth in the absence of strictures, in contrast to a 60% stricture rate encountered with tubular conduits. These results are in agreement with previous investigations using acellular SIS implants for the repair of focal and segmental defects (17, 18) suggesting that the unoperated esophageal wall parallel to the scaffold integration site plays a key role in maintaining esophageal continuity during tissue regeneration.

After 3 months of BLSF scaffold implantation, both onlay and tubular surgical models resulted in *de novo* tissues with a stratified, squamous epithelium buttressed by a vascularized lamina propria containing a mature muscularis mucosa similar to NSC. Vascular density was significantly elevated in patch as well as tubular neotissues relative to unoperated controls consistent with active tissue remodeling events (30, 36). An increase in the smooth to skeletal muscle ratio in regenerated muscularis externa relative to NSC was a common feature in both onlay and tubular repair settings. In contrast, the pattern of neotissue innervation was different following tubular versus patch reconstruction of esophageal defects. Specifically, tubular neotissues displayed significantly lower levels of innervation in comparison to NSC. However, onlay esophagoplasty procedures with BLSF grafts led to a similar density of SYP+ boutons as NSC throughout implant regions of similar length. It is conceivable that reinnervation of tubular graft sites is less efficient than patch implants due to the diminished contact area between the graft-host interface which may have slowed the rate of host neuronal integration into tubular neotissues. In addition, deficiencies in *de novo* innervation may explain the paucity of animals which exhibited peristaltic contractions following tubular esophagoplasty. Indeed, neoconduit functional assessments revealed muted off contractile responses after EFS, unlike the hypercontractile responses of patch regenerated tissues (30). However, it is still unknown if deficits in tubular neotissue peristalsis are solely due to incomplete innervation from variations in scaffold geometry, since stenting itself has been reported to negatively impact this parameter in hollow organs from trauma (39, 40).

The results of our current work demonstrate that acellular, tubular BLSF implants are permissive for *de novo* formation of esophageal tissues when used in combination with transient stenting. All neotissues examined were composed of innervated, vascularized epithelial and muscular components capable of contractile and relaxation responses and in several cases, reconstructed conduits supported oral food consumption without incidence. Tubular BLSF grafts also elicited minimal immune reactions and maintained the initial integrity of implantation sites. However, complications with our graft technology including strictures, suboptimal innervation, and sparse peristaltic function necessitate improvements in our prototype scaffold configuration and/or surgical approach. Future

studies will address several key limitations in our current experimental design. In particular, additional control groups including unoperated swine receiving stents alone or those subjected to esophagectomy and then re-anastomosed without scaffold implantation are necessary to determine if complications such as deficiencies in neotissue peristalsis and stricture formation are a consequence of surgical procedures, stenting, or implantation of the BLSF graft itself. We will also investigate if transient stenting periods >2 months significantly reduce the current rate of stricture formation after tubular esophagoplasty with BLSF matrices. Finally, we will assess the efficacy of our scaffold design to heal tubular esophageal defects >3 cm in length since these types of long-gap abnormalities cannot be repaired by primary anastomosis and currently require reconstruction with autologous tissue grafts with significant risk of complications (41). In conclusion, BLSF scaffolds represent promising platforms for tubular esophagoplasty and may offer a viable substitute for conventional surgical approaches following further experimentation and development.

Acknowledgments

This research was supported by NIH/NIDDK R01 DK107568 (JRM) and DVA BX001790 (MPS). We also acknowledge the Tufts University, Tissue Engineering Resource Center, NIH/NIBIB P41 EB002520 (Dr. David L. Kaplan, Ph.D.), for procurement of silkworm cocoons and Dr. Arthur Nedder, D.V.M. at Boston Children's Hospital for helpful discussions and technical assistance. J.R.M., K.A., and G.G. conceived and designed the experiments. G.G., D.M., V.C., M.P.S., K.A., X.Y., K.C., and C.G.A. performed the experiments. All authors executed study outcome analyses, processed and evaluated data. V.C. and J.R.M. performed statistical analyses. J.R.M., G.G., and V.C. wrote the article. All authors edited the article for conceptual and technical content. J.R.M. coordinated and supervised all aspects of the study.

Conflict of interest

The authors declare no conflicts of interest.

References

1. Menon, P., and Rao, K.L. Esophageal surgery in newborns, infants and children. *Indian J Pediatr.* **75**, 939, 2008.
2. Perry, K.A., and Merritt, R.E. Management of Barrett's esophagus and early esophageal cancer: update on endoscopic treatment strategies. *Minerva Chir.* **69**, 337, 2014.
3. Correa, C., Mallarino, C., Peña, R., Rincón, L.C., Gracia, G., Zarante, I. Congenital malformations of pediatric surgical interest: prevalence, risk factors, and prenatal diagnosis between 2005 and 2012 in the capital city of a developing country. Bogotá, Colombia. *J Pediatr Surg.* **49**, 1099, 2014.
4. Brosens, E., Ploeg, M., van Bever, Y., Koopmans, A.E., Ijsselstijn, H., Rottier, R.J., et al. Clinical and etiological heterogeneity in patients with tracheo-esophageal malformations and associated anomalies *J Thorac Dis.* **6**, S253, 2014.
5. D'Journo, X.B., and Thomas, P.A. Current management of esophageal cancer. *Eur J Med Genet.* **57**, 440, 2014.
6. Bradshaw, C.J., Sloan, K., Morandi, A., Lakshminarayanan, B., Cox, S.G., Millar, A.J.W., et al. Outcomes of Esophageal Replacement: Gastric Pull-Up and Colonic Interposition Procedures. *Eur J Pediatr Surg.* **28**, 22, 2018.
7. Bonavina, L., Via, A., Incarbone, R., Saino, G., Peracchia, A. Results of surgical therapy in patients with Barrett's adenocarcinoma. *World J Surg.* **27**, 1062, 2003.
8. Bedirli, A., Ferahkose, Z., Kerem, M., Azili, C., Sozuer, E.M., Akin, M. Comparison of free jejunal graft with gastric pull-up reconstruction after resection of hypopharyngeal and cervical esophageal carcinoma. *Dis Esophagus* **21**, 340, 2008.
9. Tannuri, U., Tannuri, A.C., Gonçalves, M.E., Cardoso, S.R. Total gastric transposition is better than partial gastric tube esophagoplasty for esophageal replacement in children. *Dis Esophagus.* **21**, 73, 2008.
10. Chang, S.Y., and Chu, P.Y. Reconstruction of the hypopharynx after surgical treatment of squamous cell carcinoma. *J Chin Med Assoc.* **72**, 351, 2009.

11. Yu, Z.K., He, S.B., Sun, J.W., Wang, Y.F., Hu, Y.M., Ping, Q., et al. Complication following gastric pull-up reconstruction for advanced hypopharyngeal or cervical esophageal carcinoma: A 20-year review in a Chinese institute. *Am J Otolaryngol.* **32**, 275, 2011.
12. Sroka, M., Wachowiak, R., Losin, M., Szlagatys-Sidorkiewicz, A., Landowski, P., Czauderna, P., et al. The Foker technique (FT) and Kimura advancement (KA) for the treatment of children with long-gap esophageal atresia (LGEA): lessons learned at two European centers. *Eur J Pediatr Surg.* **23**, 3, 2013.
13. Arakelian, L., Kanai, N., Dua, K., Durand, M., Cattan, P., Ohki, T. Esophageal tissue engineering: from bench to bedside. *Ann N Y Acad Sci.* **1434**, 156, 2018.
14. Natsume, T., Ike, O., Okada, T., Takimoto, N., Shimizu, Y., Ikada, Y. Porous collagen sponge for esophageal replacement. *J Biomed Mater Res.* **27**, 867, 1993.
15. Takimoto, Y., Teramachi, M., Okumura, N., Nakamura, T., Shimizu, Y. Relationship between stenting time and regeneration of neoesophageal submucosal tissue. *ASAIO J.* **40**, 793, 1994.
16. Yamamoto, Y., Nakamura, T., Shimizu, Y., Matsumoto, K., Takimoto, Y., Kiyotani, T., et al. Intrathoracic esophageal replacement in the dog with the use of an artificial esophagus composed of a collagen sponge with a double-layered silicone tube. *J Thorac Cardiovasc Surg.* **118**, 276, 1999.
17. Badylak, S., Meurling, S., Chen, M., Spievack, A., Simmons-Byrd, A. Resorbable bioscaffold for esophageal repair in a dog model. *J Pediatr Surg.* **35**, 1097, 2000.
18. Lopes, M.F., Cabrita, A., Ilharco, J., Pessa, P., Paiva-Carvalho, J., Pires, A., et al. Esophageal replacement in rat using porcine intestinal submucosa as a patch or a tube-shaped graft. *Dis Esophagus* **19**, 254, 2006.
19. Nakase, Y., Nakamura, T., Kin, S., Nakashima, S., Yoshikawa, T., Kuriu, Y., et al. Intrathoracic esophageal replacement by in situ tissue-engineered esophagus. *J Thorac Cardiovasc Surg.* **136**, 850, 2008.
20. Doede, T., Bondartschuk, M., Joerck, C., Schulze, E., Goernig, M. Unsuccessful alloplastic esophageal replacement with porcine small intestinal submucosa. *Artif Organs.* **33**, 328, 2009.

21. Saxena, A.K., Baumgart, H., Komann, C., Ainoedhofer, H., Soltysiak, P., Kofler, K., et al. Esophagus tissue engineering: in situ generation of rudimentary tubular vascularized esophageal conduit using the ovine model. *J Pediatr Surg.* **45**, 859, 2010.
22. Poghosyan, T., Sfeir, R., Michaud, L., Bruneval, P., Domet, T., Vanneaux, V., et al. Circumferential esophageal replacement using a tube-shaped tissue-engineered substitute: An experimental study in minipigs. *Surgery.* **158**, 266, 2015.
23. Catry, J., Luong-Nguyen, M., Arakelian, L., Poghosyan, T., Bruneval, P., Domet, T., et al. Circumferential Esophageal Replacement by a Tissue-engineered Substitute Using Mesenchymal Stem Cells: An Experimental Study in Mini Pigs. *Cell Transplant.* **26**, 1831, 2017.
24. Jensen, T., Wanczyk, H., Sharma, I., Mitchell, A., Sayej, W.N., Finck, C. Polyurethane scaffolds seeded with autologous cells can regenerate long esophageal gaps: An esophageal atresia treatment model. *J Pediatr Surg.* **54**, 1744, 2019.
25. La Francesca, S., Aho, J.M., Barron, M.R., Blanco, E.W., Soliman, S., Kalenjian, L., et al. Long-term regeneration and remodeling of the pig esophagus after circumferential resection using a retrievable synthetic scaffold carrying autologous cells. *Sci Rep.* **7**, 4123, 2018.
26. Kim, I.G., Wu, Y., Park, S.A., Cho, H., Choi, J.J., Kwon, S.K., et al. Tissue-Engineered Esophagus via Bioreactor Cultivation for Circumferential Esophageal Reconstruction. *Tissue Eng Part A.* **25**, 1478, 2019.
27. Takeoka, Y., Matsumoto, K., Taniguchi, D., Tsuchiya, T., Machino, R., Moriyama, M., et al. Regeneration of esophagus using a scaffold-free biomimetic structure created with bio-three-dimensional printing. *PLoS One* **23**, e0216174, 2019.
28. Seth, A., Chung, Y.G., Gil, E.S., Tu, D., Franck, D., Di Vizio, D., Adam, R.M., Kaplan, D.L., Estrada, C.R. Jr, Mauney, J.R. The performance of silk scaffolds in a rat model of augmentation cystoplasty. *Biomaterials* **34**, 4758, 2013.
29. Algarrahi, K., Franck, D., Ghezzi, C.E., Cristofaro, V., Yang, X., Sullivan, M.P., et al. Acellular bi-layer silk fibroin scaffolds support functional tissue regeneration in a rat model of onlay esophagoplasty. *Biomaterials* **53**: 149, 2015.

30. Algarrahi, K., Franck, D., Cristofaro, V., Yang, X., Savarino, A., Affas, S., et al. Bi-layer silk fibroin grafts support functional tissue regeneration in a porcine model of onlay esophagoplasty. *J Tissue Eng Regen Med.* **12**, e894, 2018.
31. Algarrahi, K., Franck, D., Savarino, A., Cristofaro, V., Yang, X., Affas, S., Schäfer, F.M., Sullivan, M.P. et al. Bilayer silk fibroin grafts support functional oesophageal repair in a rodent model of caustic injury. *J Tissue Eng Regen Med.* **12**, e1068, 2018.
32. Brown, B.N., Badylak, S.F. Extracellular matrix as an inductive scaffold for functional tissue reconstruction. *Transl Res.* **163**, 268, 2014.
33. Ceonzo, K., Gaynor, A., Shaffer, L., Kojima, K., Vacanti, C.A., Stahl, G.L. Polyglycolic acid-induced inflammation: role of hydrolysis and resulting complement activation. *Tissue Eng.* **12**, 301, 2006.
34. Mauney, J.R., Cannon, G.M., Lovett, M.L., Gong, E.M., Di Vizio, D., Gomez, P., Kaplan, D.L., Adam, RM. et al. Evaluation of gel spun silk-based biomaterials in a murine model of bladder augmentation. *Biomaterials.* **32**, 18, 2011.
35. Affas, S., Schäfer, F.M., Algarrahi, K., Cristofaro, V., Sullivan, M.P., Yang, X., et al. Augmentation Cystoplasty of Diseased Porcine Bladders with Bi-Layer Silk Fibroin Grafts. *Tissue Eng Part A* **25**, 855, 2019.
36. Zawicki, D.F., Jain, R.K., Schmid-Schoenbein, G.W., et al. Dynamics of neovascularization in normal tissue. *Microvasc Res.* **21**, 27, 1981.
37. Ziegler, A., Gonzalez, L., Blikslager, A. Large Animal Models: The key to translational discovery in digestive disease research. *Cell Mol Gastroenterol Hepatol.* **2**, 716, 2016.
38. Gerstein, A.D., Phillips, T.J., Rogers, G.S., Gilchrest, B.A. Wound healing and aging. *Dermatol Clin.* **11**, 749, 1993.
39. Patel, U., Kellett, M.J. Ureteric drainage and peristalsis after stenting studied using colour Doppler ultrasound. *Br J Urol.* **77**, 530, 1996.
40. Freeman, R.K., Ascioti, A.J., Dake, M., Mahidhara, R.S. An assessment of the optimal time for removal of esophageal stents used in the treatment of an esophageal anastomotic leak or perforation. *Ann Thorac Surg.* **100**, 422, 2015.

41. Bairdain, S., Zurakowski, D., Vargas, S.O., Stenquist, N., McDonald, M., Towne, M.C., et al. Long-Gap esophageal atresia is a unique entity within the esophageal atresia defect spectrum. *Neonatology*. **111**, 140, 2017.

Figure Legends

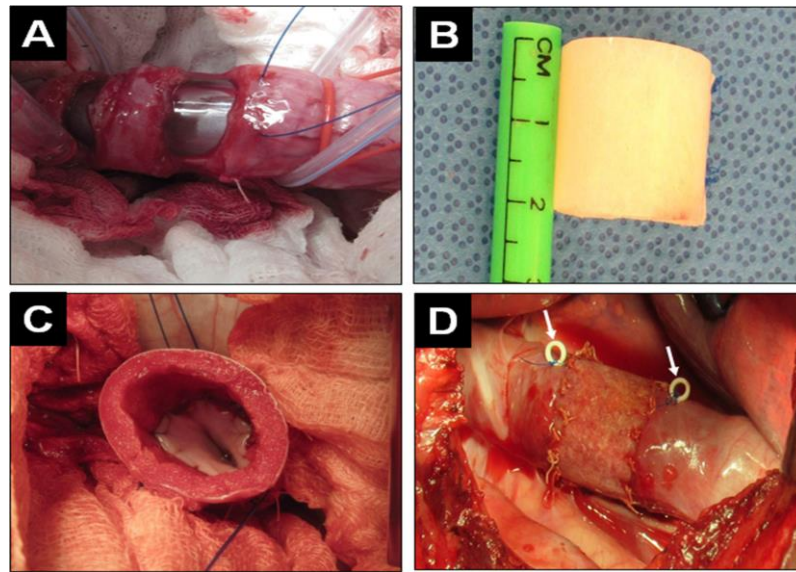


Figure 1. Tubular Esophagoplasty Procedure. [A] Exposure and resection of thoracic esophageal tissue. [B] Gross image of BLSF graft prior to surgery. [C] Anastomosis of BLSF matrix showing internal scaffold structure. [D] Complete implantation of tubular BLSF implant into the esophageal defect site. White arrows denote radio-opaque marking sutures.

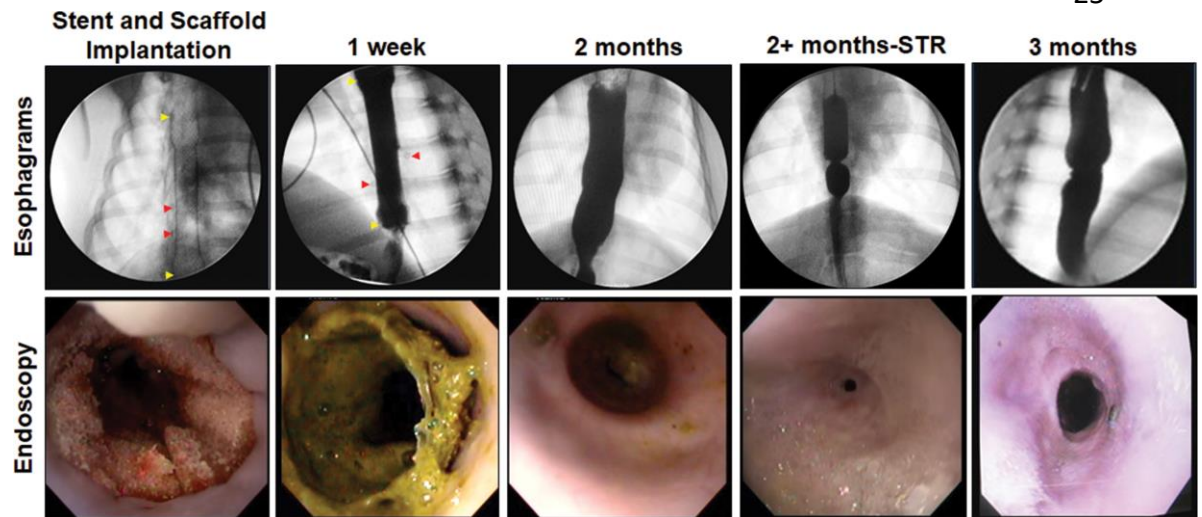


Figure 2. Radiologic imaging and esophagoscopy evaluations of reconstructed esophageal conduits. Representative data for Pigs 1-5. Esophagi were reconstructed with tubular BLSF grafts and tethered stents were placed at time of matrix implantation. Stents were removed at 2 months post-op and animals were harvested at 3 months. In some cases, stricture (STR) formation occurred between 2-3 months following biomaterial repair and neoconduits were dilated relative to surrounding tissue. Barium esophagrams of matrix-grafted swine (top row) and endoscopic assessments (bottom row) at various experimental timepoints are displayed. Yellow arrowheads mark stent boundaries. Red arrowheads annotate the radio-opaque marking sutures where visible.

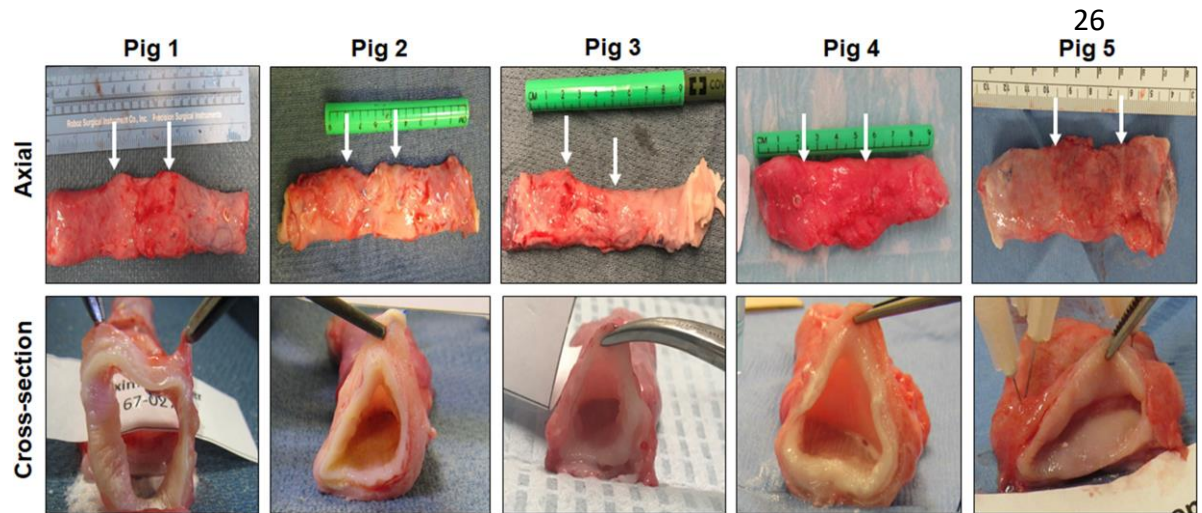


Figure 3. Necropsy assessments of esophageal neotissues at implant sites.

Photomicrographs of axial (top row) and cross-sectional (bottom row) views of neoconduits from original biomaterial graft sites in Pigs 1-5 after 3 months of implantation. Arrows denote axial marking sutures from anastomotic borders. Cross-sectional images of neotissues were taken through the central longitudinal axis.

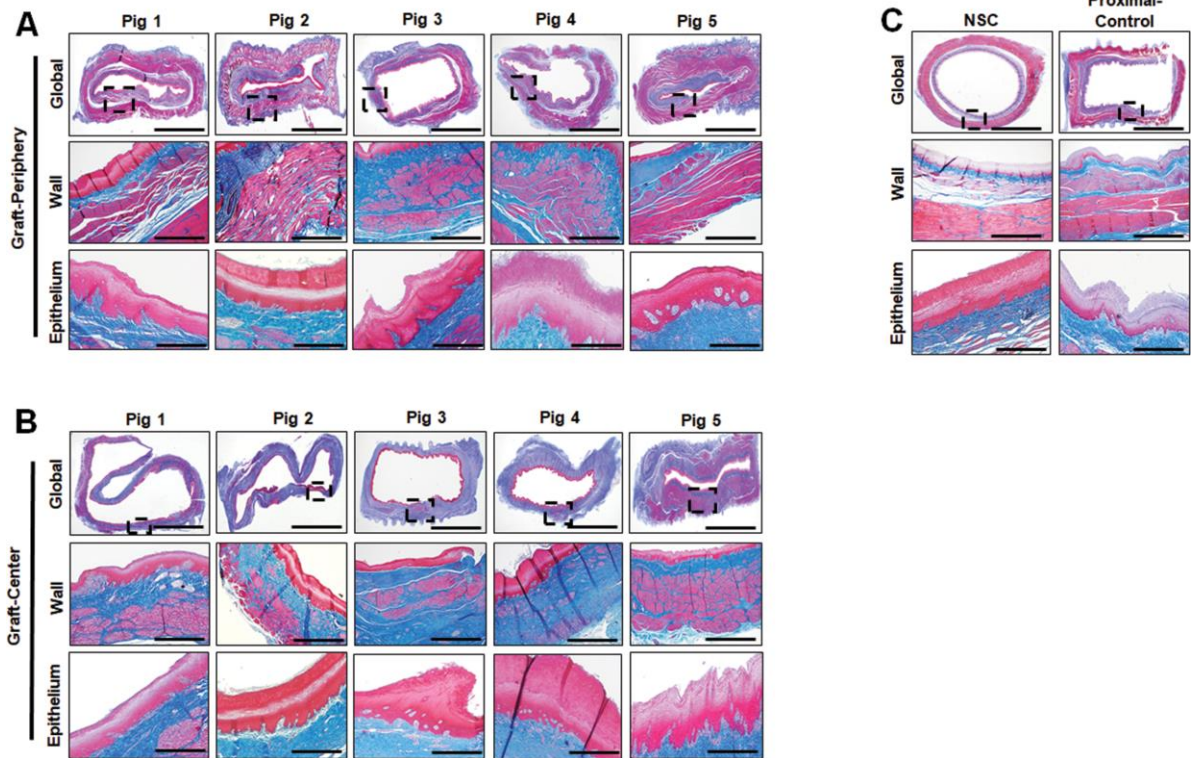


Figure 4. Histological evaluations of esophageal tissue structure in controls and neotissues. Photomicrographs of peripheral [A] and central [B] neotissue regions at 3 months post-op as well as nonsurgical controls (NSC) and proximal controls in [C] stained with MTS. Gross esophageal cross-sections are displayed in top rows with magnified views of the esophageal wall (boxed) presented in the second row of all panels. The third row in all panels displays a magnified view of the epithelium. Scale bars for photomicrographs in first, second, and third rows in all panels are 0.5 cm, 0.1 cm, and 0.02 cm respectively. Asterisk notes residual scaffold fragments. Representative data for Pigs 1-5.

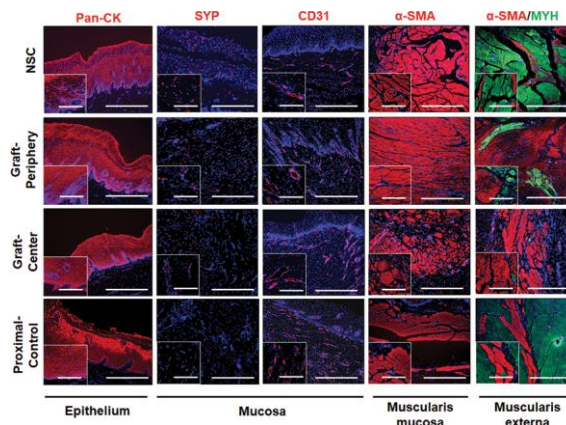


Figure 5. Immunohistochemical analyses of regenerated and control esophageal tissues. Photomicrographs of protein expression in nonsurgical controls (NSC), proximal controls, and graft regions at 3 months post-op of epithelial pan-CK (cytokeratin); innervation and endothelial makers, SYP and CD31 in mucosa; and contractile muscle markers, α -SMA and MYH in muscularis mucosa and muscularis externa. For all panels, respective marker expression is labeled in red (Alexa Fluor 594 labeling) or green (Alexa Fluor 488 labeling) with DAPI nuclear counterstain displayed in blue. Insets display magnified views of main photomicrograph. Scale bars in all main photomicrographs are 400 μ m while scale bars in insets are 150 μ m. Representative results for Figs 1-5.

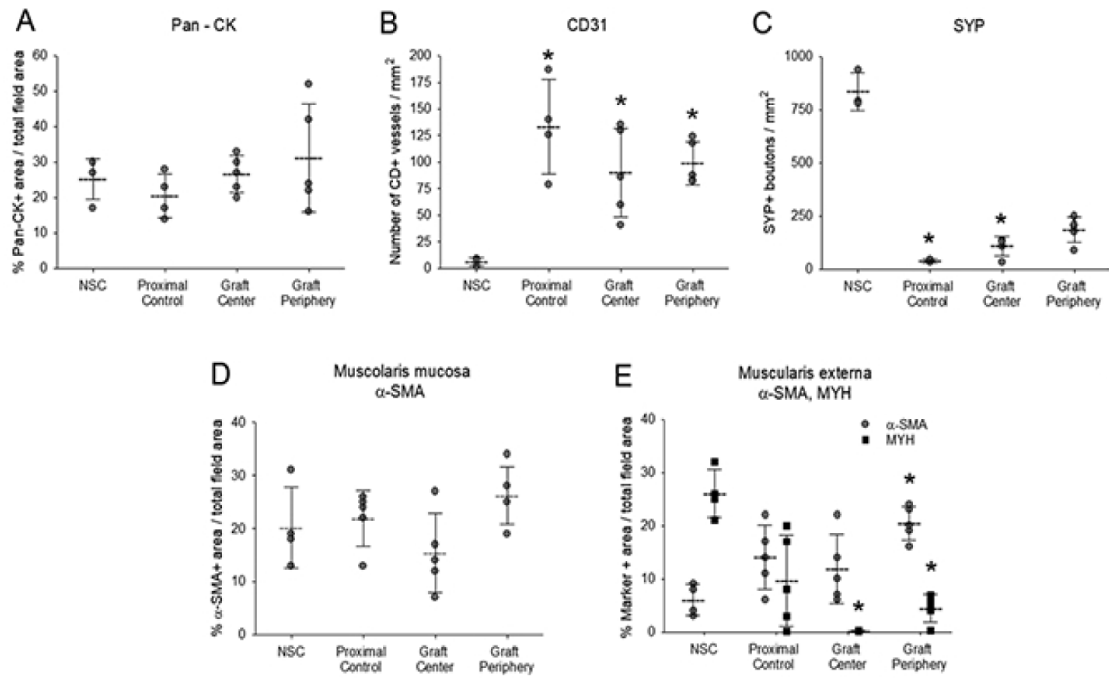


Figure 6. Histomorphometric analyses of neoconduit maturation and control tissues. [A-E] Quantitative assessments of marker expression displayed in central and peripheral regions of neotissues at 3 months post-op as well as unoperated proximal controls and nonsurgical controls (NSC). Representative data for Pigs 1-5. Symbols are individual animals. Dotted lines and error bars are mean and standard deviation, respectively. (*) = $p < 0.05$ in comparison to respective NSC levels. N=3-5 samples per data point. Results from all groups were analyzed with Kruskal-Wallis test and post hoc Dunn's test versus NSC

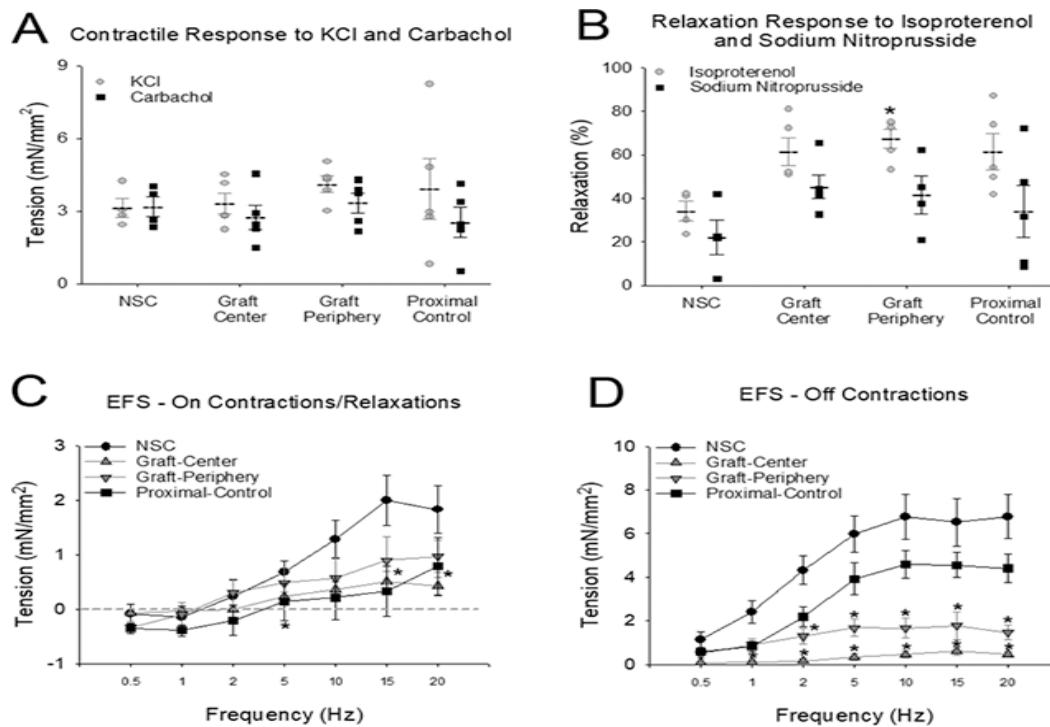


Figure 7. Ex vivo isometric tension studies in control and regenerated esophageal tissues. Quantitative evaluations of contractile and relaxation responses following agonist treatment in central and peripheral regions of neotissues at 3 months post-reconstruction as well as unoperated proximal controls and nonsurgical controls (NSC). Representative data for Figs 1-5. **[A]** Peak amplitude of contractile responses to KCl and carbachol. **[B]** Relaxation responses to isoproterenol and nitroprusside in tissues precontracted with carbachol. Data are expressed as percent of relaxation from the pre-contracted state. Symbols are individual animals. Dotted lines and error bars are mean and standard error. (*) = $p < 0.05$ in comparison to NSC levels. **[C]** The amplitudes of ON-stimulus contraction (positive values) and relaxation responses (negative values below dashed line) induced by 10 seconds of EFS at frequencies from 0.5 to 20 Hz. (*) = $p < 0.05$ in comparison to NSC. **[D]** Frequency-response curves generated from the amplitude of OFF-contractions that occur post-EFS. (*) = $p < 0.05$ in comparison to NSC. $N = 3-5$ samples per data point. Results from all groups were analyzed with Kruskal-Wallis test and post hoc Dunn's test versus NSC.

Table 1: Experimental Strategy and Outcomes for Pigs A-E.

Animal (Gender)	Type of procedure and stent strategy	Approach	Complications and management	Pre/post-op weight (kg)	Implantation period (days)	Terminal Outcomes
Pig A (Female)	Esophagoplasty + gastrostomy	G-tube feeding for first week post-op followed by oral feeding until harvest.	Stricture at the central graft site detected at 5 weeks post-op and managed with balloon dilation. Stricture recurrence observed weekly and managed with balloon dilations (7 total) until harvest.	33.2 / 34.4	120	Endoscopy and esophagram revealed recurrence of stricture in the center of graft region. No peristaltic contractions noted in neotissue.
Pig B (Female)	Esophagoplasty + untethered stent + gastrostomy	G-tube feeding for first week post-op	Stricture at the central graft site detected at 5 weeks	31.4 / 33.1	99	Tissue ingrowth into the stent prevented

		followe d by oral feeding until harvest. Stent remove d at 1 month post-op.	post-op and was managed with a single balloon dilation. New stent was placed and maintained until harvest.			imaging assessmen ts of neotissue.
Pig C (Femal e)	Esophagoplas ty + untethered stent + gastrostomy	G-tube feeding for first week post-op followe d by oral feeding until harvest. Primary stent remove d at 1 month post-op and	Stent migration into the stomach was observed at 2 months post-op.	29.1 / 30.8	101	Endoscopy and esophagra m revealed presence of stricture in the center of graft region. Peristaltic contractio ns noted in neotissue.

			replace d with seconda ry stent.			
Pig D (Femal e)	Esophagoplas ty + untethered stent + gastrostomy	G-tube feeding for first week post-op followe d by oral feeding until harvest. Primary stent remove d at 1 month post-op and replace d with seconda ry stent.	Stent migration into the stomach was observed at 2 months post-op.	36.9 / 34.8	93	Endoscopy and esophagra m revealed presence of stricture in the center of graft region. Peristaltic contractio ns noted in neotissue.

Pig E (Male)	Esophagoplas ty + untethered stent + gastrostomy	G-tube feeding for first week post-op followe d by oral feeding until harvest. Primary stent remove d at 1 month post-op and replace d with seconda ry stent.	Stent migration into the stomach was observed at 2 months post-op. Severe dysphagia noted. Early euthanasia performed.	41.7 / 41.8	60	Endoscopy and esophagra m revealed presence of stricture in the center of graft region. Severe dysphagia noted.
-----------------	--	--	--	----------------	----	--

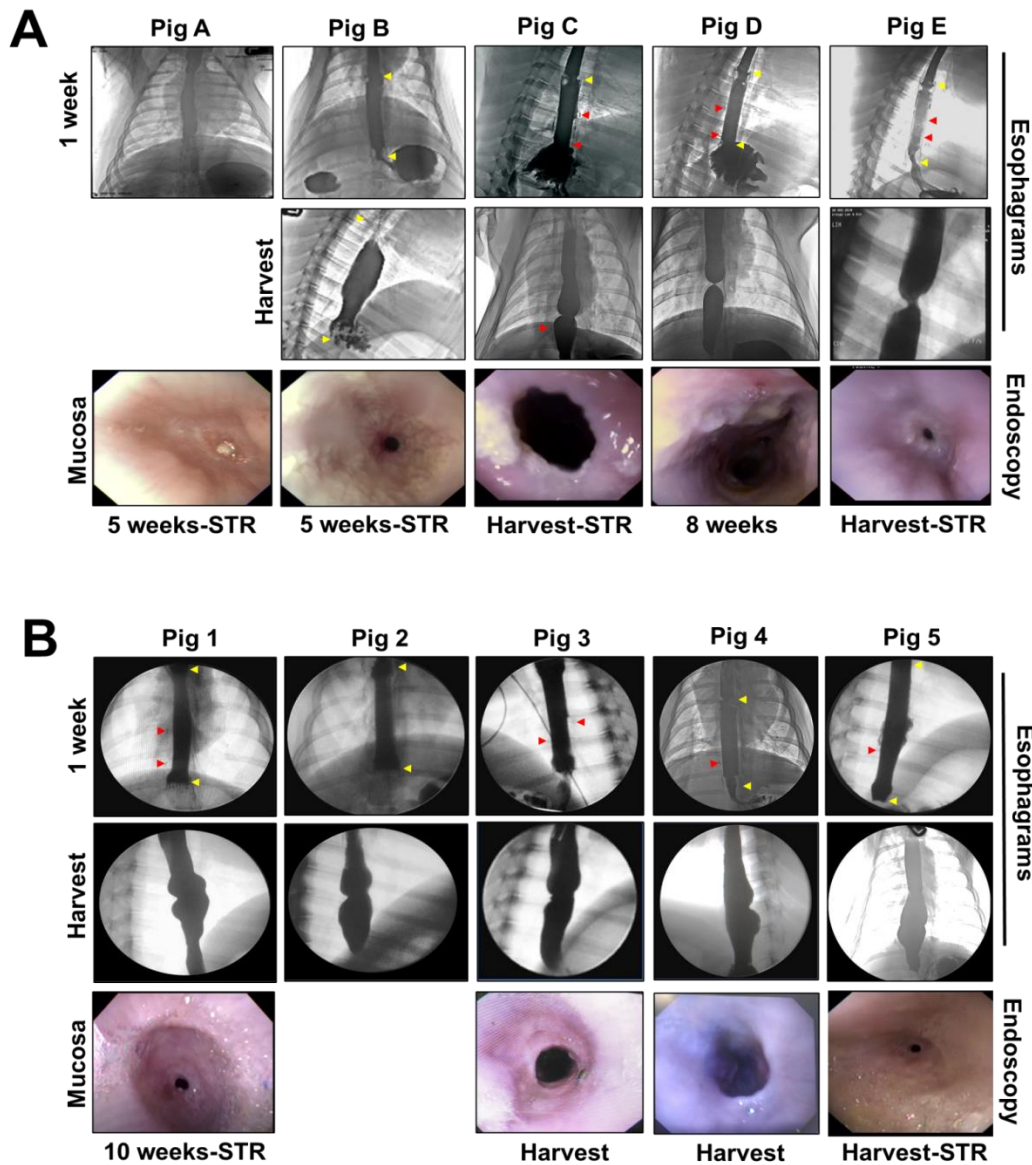
Table 2: Experimental Strategy and Outcomes for Pigs 1-5.

Animal (Gender)	Type of procedure and stent strategy	Approach	Complications and management	Pre/post-op weight (kg)	Implantation period (days)	Terminal Outcomes
Pig 1 (Female)	Esophagoplasty + suture tethered stent + gastrostomy	G-tube feeding for first week post-op followed by oral feeding until harvest. Stent removed at 2 months post-op.	Stricture at the central graft site detected 2 weeks after stent removal and was managed with a single balloon dilation.	33.7 / 33.7	88	Endoscopy revealed normal mucosa. Esophagram showed mild dilation of graft area. No peristaltic contractions noted in neotissue.

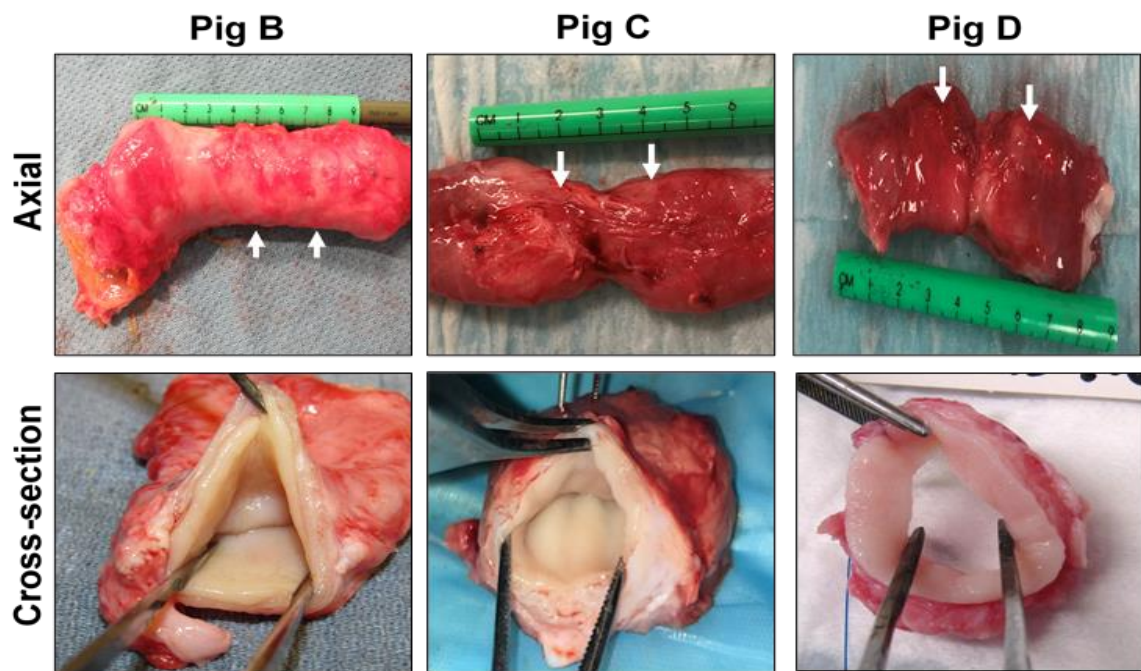
Pig 2 (Female)	Esophagoplasty + suture tethered stent + gastrostomy	G-tube feeding for first week post-operative followed by oral feeding until harvest. Stent removed at 2 months post-operative.	None	35.5 / 41.4	90	Endoscopy revealed normal mucosa. Esophagram showed mild dilation of graft area. No peristaltic contractions noted in neotissue.
Pig 3 (Female)	Esophagoplasty + suture tethered stent + gastrostomy	G-tube feeding for first week post-operative followed by oral feeding until	Stricture at the central graft site detected 2 weeks after stent removal and was managed with	29.3 / 28.1	101	Endoscopy revealed normal mucosa. Esophagram showed mild dilation of graft area. No

		harvest	balloon			peristaltic
		. Stent	dilation.			contractio
		remove	Stricture			ns noted
		d at 2	recurrence			in
		months	observed at			neotissue.
		post-	4 weeks			
		op.	following			
			stent			
			removal			
			and was			
			treated			
			with a			
			second			
			balloon			
			dilation.			
Pig 4 (Female)	Esophagopl asty + suture tethered stent + gastrostomy	G-tube feeding for first week post-op followe d by oral feeding until harvest . Stent remove	None	31.3 / 32.2	84	Endoscopy revealed normal mucosa. Esophagra m showed mild dilation of graft area. No peristaltic contractio ns noted

			d at 2 months post- op.				in neotissue.
Pig 5 (Female)	Esophagoplasty + suture tethered stent + gastrostomy	G-tube feeding for first week post-op followed by oral feeding until harvest . Stent remove d at 2 months post- op.	Stricture at the top stent flare position detected 2 weeks after stent removal and was managed with a single balloon dilation.	36.7 / 31.6	101	Endoscopy and esophagram revealed recurrence of mild stricture at the top stent flare position. Graft region was dilated and displayed peristaltic contractions.	



Supplementary Figure S1. Radiologic imaging and esophagoscopy evaluations of pilot and study group replicates. [A] Pigs A-E and [B] Pigs 1-5. Barium esophagrams of matrix-grafted swine at 1 week (top row) and 1 month (second row) post-op in both panels. Endoscopic assessments (bottom row) at various experimental timepoints are displayed. STR defines the presence of a stricture during analysis. Yellow arrowheads mark stent boundaries. Red arrowheads annotate the radio-opaque marking sutures where visible.



Supplementary Figure S2. Necropsy assessments of esophageal neotissues in pilot Pigs B-D. Photomicrographs of axial (top row) and cross-sectional (bottom row) views of neoconduits from original biomaterial graft sites in Pigs B-D following harvest. Arrows denote anastomotic borders. Cross-sectional images of neotissues were taken through the central longitudinal axis.